Resonant tunneling of charge carriers in GaAs/AlAs semiconductor heterostructure with consideration to microscopic effects

E.V. Domoratskii[1*], M.V. Zakharchenko[1], G.F. Glinskii[1]

[1]Saint-Petersburg State Electrotechnical University «LETI», Saint-Petersburg 197376, Russia

*corresponding author: evdomoratskii@gmail.com

Abstract: In this work, a mathematical model is being developed that enables the analysis of resonant tunneling of charge carriers in various multi-layered structures. The developed approach, which takes into account the charge carriers energy dispersion relation and the effect of the microscopic structure of barriers, is used to calculate the energy dependences of the tunneling coefficient, voltage-ampere characteristics, and probability density distribution for multi-barrier structures based on binary semiconductor compounds $A^{III}B^{V}$ and their solid solutions.

Introduction. Recently, there has been a great interest in electronic and spintronic nanoscale devices working on the effects of resonant tunneling. Their development and design supply humanity with high-frequency electronics on $A^{III}B^{V}$-semiconductors and heterostructures [1–5].

For modeling, it's very important to take into account the charge carriers properties in the investigated materials. It's typical to use different macroscopic parameters like effective mass or permittivity to describe kinetic phenomena in semiconductors instead of investigating microscopic properties. The main disadvantage of conventional methods, such as the method of envelope functions, is the lack of consideration for the nonparabolicity of the charge carrier dispersion law in materials forming a heterostructure, as well as the neglect of short-range interface corrections at the heterostructure interface.

We present the microscopic theory of resonant tunneling of charge carriers in semiconductor heterostructures, taking into account the exact dispersion of charge carriers and the microscopic structure of potential barriers. Using the developed theory, we analyze the double GaAs/AlAs-heterostructure.

Theory. In the framework of the proposed approach, the Hamiltonian of the system is formed from the Hamiltonian of the base crystal and the term responsible for the change in the periodic crystal potential in the region of potential barriers. A purely imaginary smooth potential is introduced near the boundaries of the region under consideration to ensure the attenuation of the charge carrier wave function [6]. The analysis is carried out within the framework of biorthogonal formalism by the method of Green's functions for the inhomogeneous Schrodinger equation in the momentum representation, which makes it possible to analyze the resonant tunneling of charge carriers through heterobarriers for a wide energy range [7]. The exact solution of the Schrodinger equation by the pseudopotential method is used.

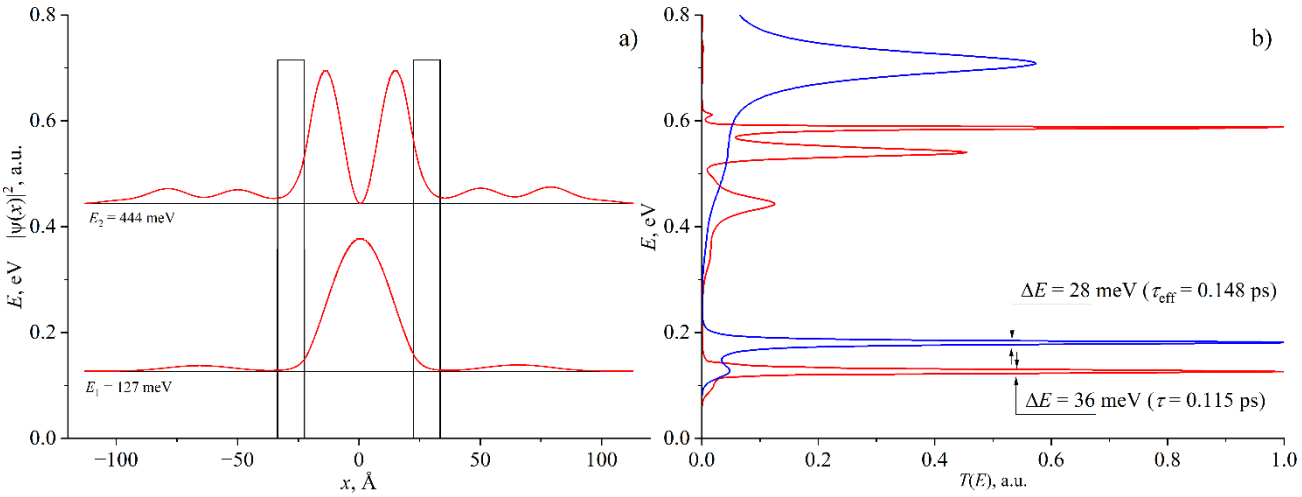

Fig. 1 Envelope wave functions (a) and energy dependence of transmission (b) (red – our theory, blue – effective mass method)

Results. A structure consisting of alternating layers of GaAs and AlAs materials is considered grown in the crystallographic direction [001]. Using developed theory were calculated the energy dependence of the tunneling coefficient and probability density distribution (Fig. 1). The tunneling time of charge carriers in the system according to the envelope function method is 0.115 ps, and according to the effective mass method – 0.148 ps, which is in good agreement with the results of studies of such a two-barrier structure [9], where the authors report the time calculated from the effective mass method equal to 0.19 ps. The difference in the tunneling time values calculated by the effective mass method is due to different modeling methods - the authors used grid methods in the coordinate representation, while in this work, the calculation was carried out in the momentum representation by solving a system of linear algebraic equations. The dwell time from the experiment [9] is 0.11 ps. As a result, the theory being developed makes it possible to more accurately calculate the characteristic tunneling time of charge carriers in the system and clarify the position of the resonant peak of the barrier transparency in the spectrum.

References

[1] Encomendero, J., Faiza, A.F., Islam, S.M., Protasenko, V., Rouvimov, S., Berardi, S.-R., Fay, P., Debdeep, J., and Huili, G. X., "New tunneling features in polar III-nitride resonant tunneling diodes", Phys. Rev. X, **7(4)**, 041017 (2017).

[2] Jauho, A. P., Wingreen, N. S., Meir, Y., "Time-dependent transport in interacting and noninteracting resonant-tunneling systems", Phys. Rev. B, **50 (8)**, 5528 (1994).

[3] Wang, J., Naftaly, M., Wasige, E., "An overview of terahertz imaging with resonant tunneling diodes", Appl. Sciences, **12(8)**, 3822 (2022).

[4] Suzuki, S., Asada, M., "Fundamentals and recent advances of terahertz resonant tunneling diodes", Appl. Phys. Express, **17**, 070101 (2024).

[5] Cimbri, D., Wang, J., Al-Khalidi, A. and Wasige, E., "Resonant tunnelling diodes high-speed terahertz wireless communications", IEEE Transactions on Terahertz Science and Technology, **12(3)**, 226–244 (2022).

[6] Zakharchenko, M.V., Glinskii, G.F., "The theory of resonant tunneling of charge carriers within the framework of the Green's function method and biorthogonal formalism", J. of Tech. Phys., **10(93)**, 1396–1400 (2023).

[7] Domoratsky, E.V., Zakharchenko, M.V., Glinskii, G.F., "Effects of resonant tunneling in GaAs/AlAs heterostructure", St. Petersburg State Polytechnical University Journal. Physics and Mathematics, **17(1.1)**, 55–61 (2024).

[9] Brown, E. R., Sollner, T. C.L.G., Parker, C.D., Goodhue, W.D., Chen, C.L., "Oscillations up to 420 GHz in GaAs/AlAs resonant tunneling diodes", Appl. Phys. Lett., **55(17)**, 1777–1779 (1989).

Nanomaterials and microresonators in laser physics: femtosecond pulse generation at extreme repetition rates

Yu. Gladush[1*], A. Netrusova[1], A. Mkrchyan[1], M. Mishevskiy[1*], D. Krasnikov[1] and A. Nasibulin[1]

[1]Skolkovo Institute of Science and Technology, the territory of the Skolkovo Innovation Center, Bolshoy Boulevard, 30, bld. 1, Moscow 121205, Russia

[*]corresponding author: y.gladush@skoltech.ru

Abstract: We propose and compare several approaches for ultrashort pulse generation in fiber laser with high pulse repetition rate. This includes erbium laser made of ionic liquid gated carbon nanotubes and integrated microring resonator nested in the fiber cavity. First approach implies harmonic mode locking, which allows to increase fundamental repetition rate of the laser tens or even hundreds of times, but suffers from low reproducibility and high pulse jitter. In contrast, lasers with nested resonators can operate on the repetition rates of the microcavities which reach 1 THz and provide reproducible pulse trains with low jitter.

Ultrafast lasers with high repetition rates are paving the road towards real world application. Among them soliton information transmission and generation of entangled photons. For some applications it is not a pulse train that it is needed, but its representation in frequency domain – a frequency comb – an equidistant sequence of narrow coherent spectral lines. Frequency combs with GHz to THz spacing may find applications in spectroscopy, coherent data transmission, coherent lidars and many more. In the work we present two approaches for high repetition rate pulse generations.

First, we consider laser with a carbon nanotube saturable absorber deposited on a side polished fiber. We show that controlling the response of a saturating absorber with electrochemical gating allows to control the pulse generation of a fiber laser. It includes switching between mode locking and Q-switching, as well as switching between different orders of harmonic mode synchronization. It is known that for lasers without polarization conservation, the order of harmonic synchronization at a given pump can significantly depend on the position of the polarization controller, while generation in a laser with polarization conservation, a given generation mode is considered more reproducible. We show that when adding another degree of freedom, the state of the saturating absorber, the order of harmonic mode locking for a given pump and the state of the absorber may depend on the trajectory along which we arrived at a given point in the parameter space of the laser. This behavior opens up opportunities for using machine learning to find optimal trajectories corresponding to the maximum harmonic mode synchronization order [1]. With this approach we demonstrate pulse repetition rates up to hundreds of MHz with possibility for further increase to GHz scale.

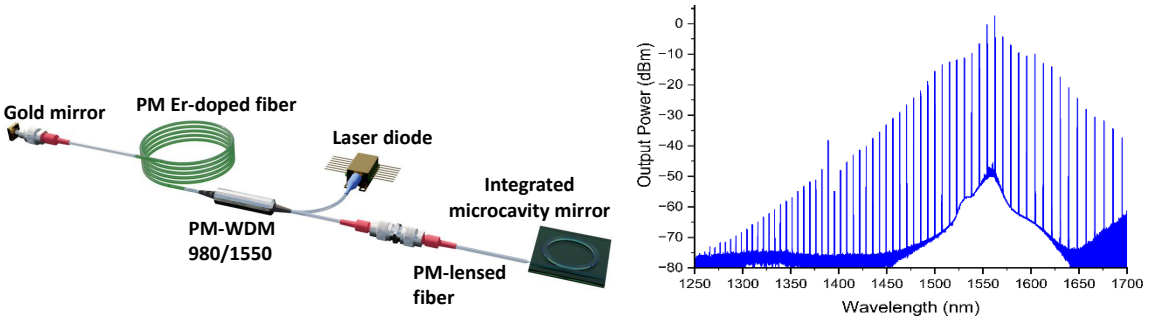

Fig. 1 (a) Scheme of the fiber laser with microring cavity (not in scale); (b) Spectrum of the optical comb on the output of laser.

To go for a much higher repetition rate it is necessary to use another technique – a so-called filter driven four wave mixing. In this technic a microring resonator is implemented into the cavity, that filters laser modes forcing the laser to generate pulses on a repetition rate of the microcavity. We suggest further development of this approach by utilizing the two-port integrated chip with microcavity working as a reflecting mirror in fiber laser resonator (see Fig. 1a). Here laser resonator is formed by the gold mirror on one side and microring resonator on the other. High quality factor microring resonator give rise to a comb formation through four wave mixing. In the ring microcavity directly propagating comb give rise to the counter propagating comb due to Rayleigh scattering, which goes back into the laser cavity forming an optical feedback. With this approach we show robust self-starting soliton comb generation with spectral width more than 500 nm, which greatly exceeds erbium amplification window (see Fig. 1b). In the time domain it gives a train of femtosecond pulses with repetition rate of the microring cavity reaching 1 THz in our experiment [2].

This work is supported by the Russian Science Foundation (Grant No. №25-22-00388)

References

[1] Kokhanovskiy, A., Kuprikov, E., Serebrennikov, K., Mkrtchyan, A., Davletkhanov, A., Bunkov, A., Krasnikov, D., Shashkov, M., Nasibulin, A. and Gladush, Y. "Multistability manipulation by reinforcement learning algorithm inside mode-locked fiber laser," Nanophotonics, Vol. 13 (Issue 16), pp. 2891-2901 (2024)

[2] Mkrtchyan A, et al. "Microring resonator as a Rayleigh mirror for broadband laser cavity comb generation," arXiv:2503.09166

Influence of epoxy components on the optical properties of single-walled carbon nanotube films and fibers

Nikita E. Gordeev[1*], Hassaan A. Butt[1], Sergei P. Shadrov[1], Vladislav A. Kondrashov[1], Anastasia E. Goldt[1], Veronika A. Dmitrieva[1], Aliya R. Vildanova[1], Dmitry V. Krasnikov[1], Albert G. Nasibulin[1]

[1]Skolkovo Institute of Science and Technology, the territory of the Skolkovo Innovation Center, Bolshoy Boulevard, 30, bld. 1, Moscow 121205, Russia

[*]corresponding author: Nikita.Gordeev@skoltech.ru

Abstract: We studied the influence of epoxy and its components on the optical properties of SWCNT films and fibers. Our study demonstrates that the hardener epoxy component is a mild (3-5cm^{-1} G-

peak Raman shift) dopant for SWCNTs, an effect we attribute to the amines present in the hardener. This doping effect was not observed after the epoxy was fully cured. This can be attributed to the chemical bonding between the hardener and the epoxy resin, which leads to negligible influence of the hardener on the SWCNTs after complete solidification.

Single-walled carbon nanotubes (SWCNT) macro-assemblies, such as films and carbon nanotube fibers (CNTFs), are promising candidates for sensing applications. They can identify and quantify stress, temperature and the liquid-to-solid transition in polymers. However, due to their sensitivity to multiple simultaneous stimuli, it is necessary to isolate and quantify the impact of each factor to delineate the causes of their response [1].

This study investigates the influence of epoxy components (resin and hardener) and the cured epoxy on the optical properties of SWCNT films and wet-pulled CNTFs using a multi-technique spectroscopic approach [3,4]. A doping effect from the amine-based epoxy hardener was observed both in SWCNT films and CNTFs [2]. Raman spectroscopy revealed mild doping in CNTFs, evidenced by ~5cm^{-1} G-peak shift. In SWCNT films, although the G-peak position did not change, a suppressed shoulder and a shift of the D-peak by ~3cm^{-1} along with its suppression by ~10% confirmed the presence of doping. This doping alters the density of states (DOS) at the Fermi level, leading to enhanced sensitivity of the SWCNT films and CNTFs to temperature [5,6]. UV-Vis-NIR spectroscopy of the SWCNT films further confirmed this doping through the suppression of the S11 and M11 transitions (by factor of ~3 and ~1.1, respectively), while simultaneously excluding the epoxy resin as a dopant. Finally, FTIR spectroscopy identified the absence of chemical interactions between SWCNTs in both films and CNTFs with the hardener after epoxy was cured.

Based on this data, we conclude that while the doping of the SWCNTs takes place with liquid hardener, amine groups in the hardener are more likely to react with resin monomers than to form chemical bonds with SWCNTs. Therefore, the polymerization process overcomes SWCNT doping that was confirmed by optical methods of characterization.

References

[1] G.V. Rogozhkin, N.E. Gordeev, H.A. Butt, V.A. Kondrashov, A.E. Goldt, V.A. Dmitrieva, A.R. Vildanova, S.D. Konev, I.V. Sergeichev, Z. Wang, J. Qi, Y. Yan, D.V. Adamchuk, S.A. Maksimenko, D.V. Krasnikov, A.G. Nasibulin, "Mechanically neutral and facile monitoring of thermoset matrices with ultrathin and highly porous carbon nanotube films", Carbon **230** 119603, (2024)

[2] J.C. Fernández‐Toribio, A. Íñiguez‐Rábago, J. Vilà, C. González, Á. Ridruejo, J.J. Vilatela, A Composite Fabrication Sensor Based on Electrochemical Doping of Carbon Nanotube Yarns, Advanced Functional Materials, **26** 7139 – 7147, (2016)

[3] M.A. Zhilyaeva, E.V. Shulga, S.D. Shandakov, I.V. Sergeichev, E.P. Gilshteyn, A.S. Anisimov, A.G. Nasibulin, "A novel straightforward wet pulling technique to fabricate carbon nanotube fibers", Carbon **150** 69–75, (2019)

[4] A. Jorio., R. Saito, Raman Spectroscopy for Carbon Nanotube Applications, Journal of Applied Physics **129 (2)** 021102, (2021)

[5] M.T.Z. Myint, T. Nishikawa, H. Inoue, K. Omoto, A.K.K. Kyaw, Y. Hayashi, Improved room-temperature thermoelectric characteristics in F4TCNQ-doped CNT yarn/P3HT composite by controlled doping, Organic Electronics **90** 106056, (2021).

[6] I. Puchades, C.C. Lawlor, C.M. Schauerman, A.R. Bucossi, J.E. Rossi, N.D. Cox, B.J. Landi, Mechanism of chemical doping in electronic-type-separated single wall carbon nanotubes towards high electrical conductivity, J. Mater. Chem. **C 3** 10256–10266, (2015).

Broadband microcomb generation using integrated high-Q microring resonator nested into fiber-cavity with gain media

A. S. Netrusova[1, *], A. A. Mkrtchyan[1], Z. Ali[1], M. S. Mishevsky[1], N. Yu. Dmitriev[2], K. N. Minkov[2], D. A. Chermoshentsev[2,3], M. A. Melkumov[4], A. G. Nasibulin[1], I. A. Bilenko[2] and Y. G. Gladush[1]

[1]*Skolkovo Institute of Science and Technology, 30 Bolshoy B*oulevard, building 1, Moscow, 121205, Russia

[2]Russian Quantum Center, 30 Bolshoy Boulevard, building 1, Skolkovo Innovation Center territory, 121205, Russia

[3]Moscow Institute of Physics and Technology, (National Research University), Dolgoprudny, 141700, Russia

[4]Fiber Optics Research Center of the Russian Academy of Sciences*, 38 Vavilov str., Moscow, 119333, Russia*

[*]corresponding author: Anastasia.Netrusova@skoltech.ru

Abstract: We demonstrate a compact hybrid fiber-laser system in which a single-bus Si_3N_4 microring functions as a nonlinear reflective element. Rayleigh backscattering forms the cavity and enables robust, self-starting single-soliton generation without additional ports or filters. By changing the fiber gain medium, the system produces broadband soliton combs across different wavelength bands: >400 nm with erbium gain and >300 nm with bismuth gain, while a hybrid Er–Bi cavity yields >400 nm bandwidth. Coupled-mode simulations reproduce stable single-soliton operation under the same conditions, confirming the underlying dynamics.

Integrated high-Q microresonators have become a key technology for compact optical frequency combs (OFCs) finding use in precision metrology[1-3], optical communications [4-6], and quantum systems[7]. Traditional soliton-based comb generation, however, is limited by low pump-to-comb conversion efficiency (<5%) and typically requires active control because the dynamics are not inherently self-starting [8]. A recent approach addressed this by embedding four-port microcavities into fiber lasers, enabling self-starting soliton combs with efficiencies up to 75%[9]. In our work, we take a different route: an integrated Si_3N_4 high-Q microring, coupled through a single bus waveguide, is used as a nonlinear reflective element inside a fiber-laser cavity (Fig. 1a). Rayleigh backscattering of the generated comb lines provides the feedback needed to form the cavity, eliminating the need for additional ports or external loops. The microring therefore plays the role of a nonlinear mirror that supports robust passive mode-locking and stable single-soliton formation [10].

A key strength of this setup is its spectral adaptability. By switching only the fiber gain medium, we can realize soliton combs in different wavelength regions. With an erbium-doped fiber, we obtain a stable, coherent soliton comb spanning more than 400 nm with ~1 ps pulses confirmed by autocorrelation and laser-scanning spectroscopy (Fig. 1b-c). In addition, we developed a numerical model based on coupled-mode equations that reproduces the experimentally observed regime and supports the formation of a stable single soliton under the same operating conditions. Using a bismuth-doped fiber, we additionally demonstrate broadband combs exceeding 300 nm (Fig. 1d). When combining Er- and Bi- fibers in a hybrid cavity, we generate a broadband comb >400 nm with comb

lines coherently linked through non-degenerate four-wave mixing in the microring (Fig. 1e). This hybrid comb is long-term stable and recovers its state after external perturbations.

Overall, our results introduce a compact and highly configurable platform for ultrafast comb generation, particularly advantageous in systems where single-port operation and wide spectral tunability are desired. The ability to employ multiple gain media within a single cavity also points toward a promising route for achieving octave-spanning spectra, as their combined gain bandwidth enables coherently bound comb formation through nonlinear interactions in the microresonator.

This work is supported by the Russian Science Foundation (Grant No. 25-22-00388).

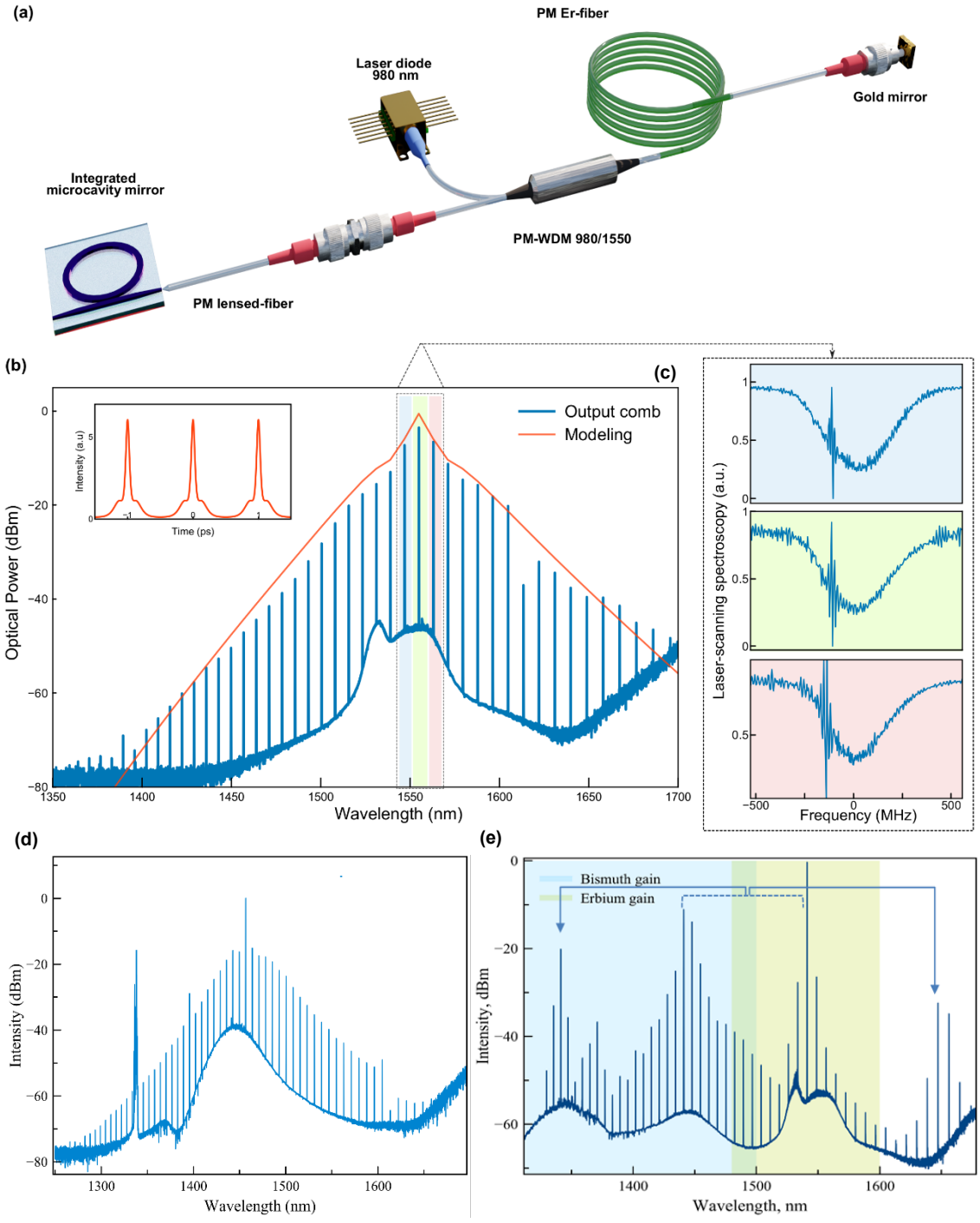

Fig. 1. Broadband frequency comb generation. (a) The setup includes a one-meter-long polarization-maintaining erbium-doped fiber, pumped by a 980 nm laser diode via a broadband 980/1550 nm wavelength-division multiplexer (PM-WDM). All fiber components are polarization-maintaining and exhibit a second-order dispersion of −23 fs²/mm. Light is coupled to the integrated photonic chip using lensed fibers. Si_3N_4 microring resonator has 1 THz repetition rate, nearly 1 million Q- factor and anomalous dispersion. (b) Measured soliton comb (blue) and model-derived intracavity spectrum (red). The simulated spectrum and pulse are shown because direct autocorrelation measurements would require amplification, which broadens the pulses and distorts the ACF. (c) Red-detuning is confirmed by laser-scanning spectroscopy of main lines within spectrum. Broadband self-starting optical frequency comb, with more than 350 nm width within (d) bismuth gain region and (e) both gain media (erbium +bismuth).

References

[1] S. B. Papp *et al.*, "Microresonator frequency comb optical clock," *Optica*, vol. 1, no. 1, p. 10, Jul. 2014, doi: 10.1364/optica.1.000010.

[2] P. Del'Haye *et al.*, "Phase-coherent microwave-to-optical link with a self-referenced microcomb," *Nat Photonics*, vol. 10, no. 8, pp. 516–520, Aug. 2016, doi: 10.1038/nphoton.2016.105.

[3] W. Liang *et al.*, "High spectral purity Kerr frequency comb radio frequency photonic oscillator," *Nat Commun*, vol. 6, Aug. 2015, doi: 10.1038/ncomms8957.

[4] P. Marin-Palomo *et al.*, "Microresonator-based solitons for massively parallel coherent optical communications," *Nature*, vol. 546, no. 7657, pp. 274–279, Jun. 2017, doi: 10.1038/nature22387.

[5] H. Hu *et al.*, "Single-source chip-based frequency comb enabling extreme parallel data transmission," *Nat Photonics*, vol. 12, no. 8, pp. 469–473, Aug. 2018, doi: 10.1038/s41566-018-0205-5.

[6] B. Corcoran *et al.*, "Ultra-dense optical data transmission over standard fibre with a single chip source," *Nat Commun*, vol. 11, no. 1, Dec. 2020, doi: 10.1038/s41467-020-16265-x.

[7] N. C. Menicucci, S. T. Flammia, and O. Pfister, "One-way quantum computing in the optical frequency comb," *Phys Rev Lett*, vol. 101, no. 13, p. 130501, Sep. 2008, doi: 10.1103/PhysRevLett.101.130501.

[8] X. Xue, P. H. Wang, Y. Xuan, M. Qi, and A. M. Weiner, "Microresonator Kerr frequency combs with high conversion efficiency," *Laser Photon Rev*, vol. 11, no. 1, Jan. 2017, doi: 10.1002/lpor.201600276.

[9] H. Bao *et al.*, "Laser cavity-soliton microcombs," *Nature Photonics 2019 13:6*, vol. 13, no. 6, pp. 384–389, Mar. 2019, doi: 10.1038/s41566-019-0379-5.

[10] A. A. Mkrtchyan *et al.*, "Microring resonator as a Rayleigh mirror for broadband laser cavity comb generation," Apr. 2025: arXiv:2503.09166.

Semiconductor nanocrystals grow rate dependency from microfluidic channel cross section

I. A. Reznik[1*], S. Bikmetova[1], and M. Zyuzin[1]

[1]School of Physics and Engineering, ITMO University, 191002 St. Petersburg, Russia

[*]corresponding author: ivan.reznik@metalab.ifmo.ru

Abstract: We investigated the photophysical properties of $AgInS_2$ quantum dots synthesized in microfluidic chips with different channel cross-sections (1 mm², 0.25 mm², and 0.0625 mm²). It was demonstrated that reducing the channel size, while keeping the total internal volume constant, accelerates quantum dot growth.

Microfluidic synthesis of semiconductor nanostructures provides a cost-effective approach for producing photosensitizers and offers improved control over their photophysical properties.

Compared to conventional batch techniques, microfluidic platforms enable precise temperature regulation, efficient mixing, and scalability, making them highly attractive for the synthesis of luminescent quantum dots [1].

In this work, microfluidic chips were fabricated using 3D-printed molds followed by PDMS replica and glass slide plasma bonding. Each chip had an internal volume of 25 µL, while the cross-sectional area of the reaction channel was varied (1 mm², 0.25 mm², and 0.0625 mm²) (Fig. 1). Owing to the small internal volume, the reaction mixture was circulated multiple times through the reactor to achieve a total thermal exposure of 30 min at 90 °C [2]. The flow rate of reagents also varied between 1, 2.5, and 10 µL/s. Photophysical characterization was performed using a Cary Eclipse spectrofluorometer, PicoQuant lifetime spectroscopy, and TEM microscopy.

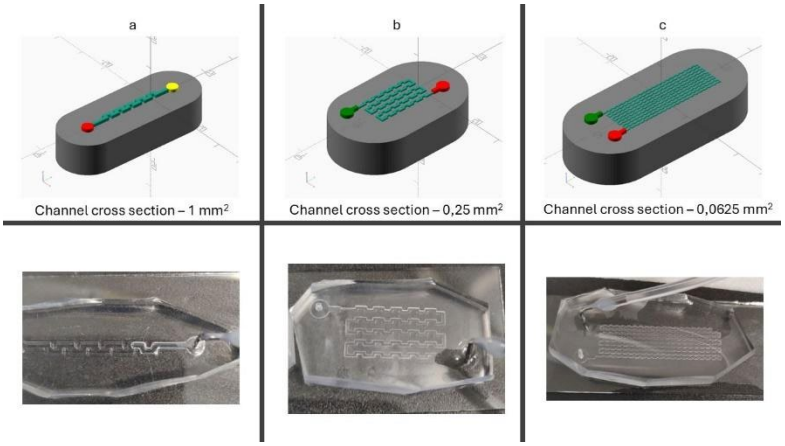

Fig. 1 (a) Schematic illustration of a chip CAD design and physical replica with channel cross section - 1, 0.25 and 0.0625 mm^2 for (a), (b) and © respectively.

Figure 2a shows a slight redshift of the emission band (≈50 nm) as the channel cross-section decreases. Luminescence decay profiles (Fig. 2b) remain nearly unchanged in shape, while lifetime analysis reveals a moderate increase in decay times for smaller channels, suggesting reduced defect density due to faster heating [3]. TEM images (Fig. 2c) confirm the formation of ~4 nm quantum dots, and histograms of size distributions (Fig. 2d) reveal a systematic increase in particle size (from 2.9 to 3.6 nm) with decreasing channel cross-section. Figure 2e presents the dependence of particle size on both channel dimension and flow rate, highlighting that at higher flow rates, the influence of channel geometry is significantly diminished.

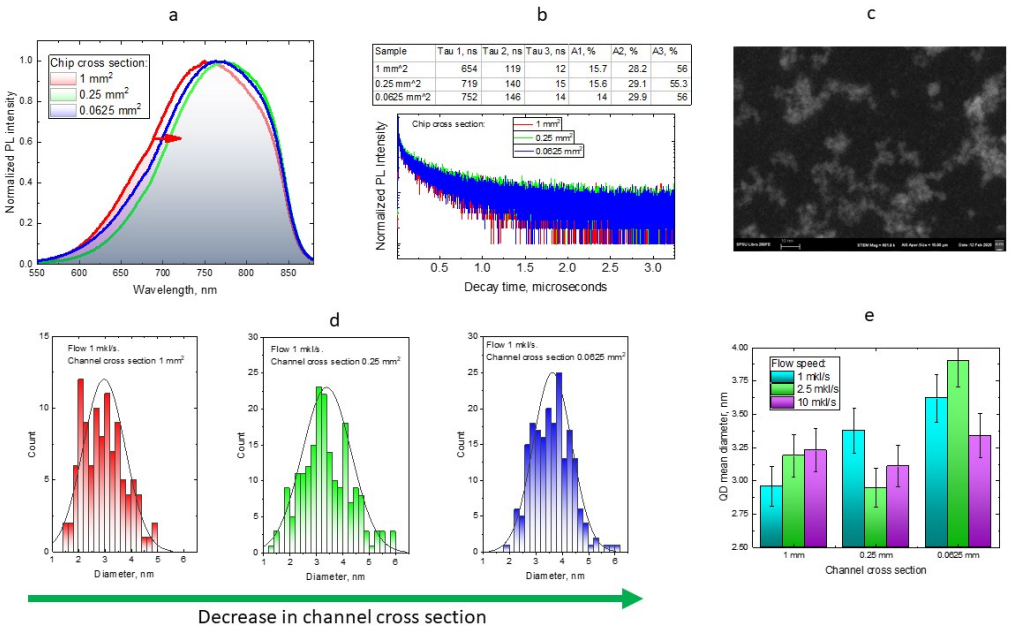

Fig. 2 (a,b) PL spectra and PL decay curves of $AgInS_2$ quantum dots synthesized in chips with different cross sections. (c) TEM images of $AgInS_2$ quantum dots synthesized in microfluidic chip with cross section 1 mm^2. (d) Size histogram of $AgInS_2$ quantum dots synthesized in chips with different cross sections. (e) $AgInS_2$ quantum dots diameter dependency from channel cross section and reagent mixture flow speed.

These results demonstrate that efficient microfluidic synthesis of $AgInS_2$ quantum dots does not require highly complex geometries or micron-scale channel dimensions. The findings suggest that even relatively simple chip designs can provide controlled growth conditions and high-quality nanocrystals, thereby facilitating scalable and accessible microfluidic approaches for luminescent materials.

This work is supported by the Russian Science Foundation (25-73-20100).

References

[1] Saeed, Muhammad Mubashar, et al. "Advances in nanoparticle synthesis assisted by Microfluidics." Lab on a Chip (2025).

[2] Ding, Caiping, et al. "Synthesis and bioapplications of Ag2S quantum dots with near-infrared fluorescence." Advanced Materials 33.32 (2021): 2007768.

[3] Chen, Ting, et al. "A review on multiple I-III-VI quantum dots: preparation and enhanced luminescence properties." Materials 16.14 (2023): 5039.

Strong coupling of chiral light with chiral matter: a macroscopic study

N. S. Salakhova[1*], S. A. Dyakov[1], I. A. Smagin[1*], I.M. Fradkin[1] and N. A. Gippius[1]

[1]Skolkovo Institute of Science and Technology, the territory of the Skolkovo Innovation Center, Bolshoy Boulevard, 30, bld. 1, Moscow 121205, Russia

[*]corresponding author: Natalia.Salakhova@skoltech.ru

Abstract: We studied the strong coupling of chiral light with chiral material by incorporating the

Lorentz pole into macroscopic chirality parameter: dielectric permittivity, magnetic permeability, and chirality coefficient. Our study demonstrates significantly distinct behaviors between the material's enantiomers, offering a promising approach for their detection and selective differentiation.

The detection and selection of chiral organic molecules with different handedness are critical for numerous applications in pharmacology, biology, and chemistry. Due to their similar size and chemical structure, the most promising approach is to exploit differences in their optical responses when interacting with an electromagnetic field. In this work, we focus on the coupling between chiral medium and chiral photonic modes within a resonator in macroscopic framework. This approach allows for the study of high molecular concentrations not accessible through microscopic analyses of chiral polaritons [1, 2].

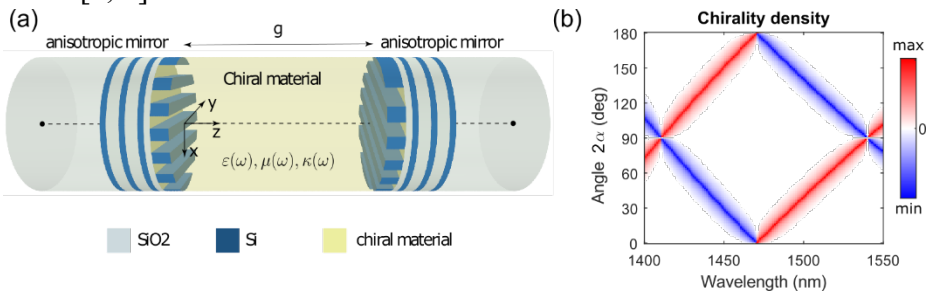

Fig. 1 (a) Schematic illustration of a chiral Fabry–Perot resonator filled with chiral material. (b) Chiral modes of an empty Fabry–Perot resonator as a function of the rotation angle between the two mirrors.

Specifically, we consider a Fabry-Perot resonator with dielectric handedness-preserving mirrors Fig.1(a). Mirrors are constructed from a combination of dielectric Bragg mirrors and a one-dimensional photonic crystal slab, forming a layer with high artificial anisotropy. The mirrors are optimized to achieve near-unity reflection and to preserve the handedness of light across a broad spectral range. This configuration enables the Fabry-Perot cavity to support photonic modes with high electromagnetic chirality for both handednesses, which separate when the rotational angle between the upper and lower mirrors deviates from integer multiples of $\pi/2$ Fig.1 (b) [3]. The resonant medium inside the cavity is described by macroscopic material parameters: dielectric permittivity, magnetic permeability, and chirality coefficient having a Lorentz pole. The mode splitting near the resonant wavelength varies depending on the value of the chirality parameter Fig.2 (a-b). At a specific value of the chirality coefficient, a particularly intriguing regime emerges, as shown in Fig. 2(c). In this case, different light–matter coupling regimes are observed depending on the handedness of the material chirality. For example, a medium with positive chirality coefficient may exhibit strong coupling with the electromagnetic field, while a medium with opposite chirality remains in a weak coupling regime.

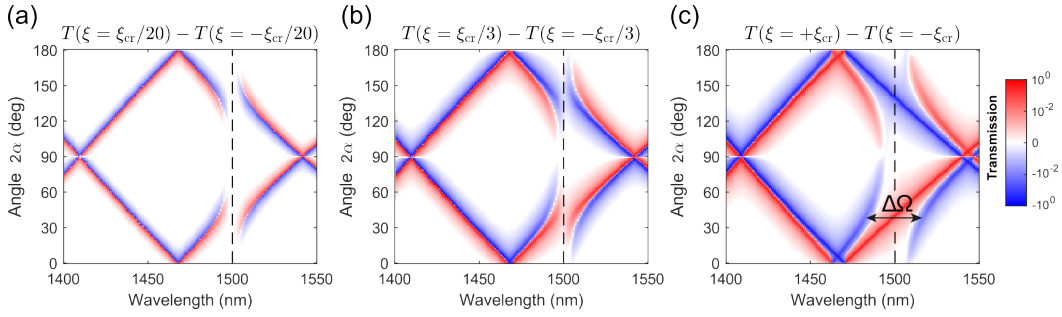

Fig. 2 Transmission spectra differences between materials of opposite handedness, shown as a function of the rotation angle. Panels (a)–(c) present results for different values of the chirality coefficient.

These findings offer exciting prospects for developing advanced methods to detect chiral molecules with different handedness.

This work is supported by the Russian Science Foundation (Grant No. 25-12-00454)

References

[1] Baranov, D. G., Schäfer, C., & Gorkunov, M. V., "Toward molecular chiral polaritons," ACS Photonics, **10(8)**, 2440-2455 (2023).

[2] Riso, R. R., Castagnola, M., Ronca, E., & Koch, H., "Chiral polaritonics: cavity-mediated enantioselective excitation condensation,' Rep. Prog. Phys., **88(2)**, 027901 (2025).

[3] Dyakov, S. A., Salakhova, N. S., Ignatov, A. V., Fradkin, I. M., Panov, V. P., Song, J. K., & Gippius, N. A, "Chiral light in twisted fabry–pérot cavities," AOM, **12(12)**, 2302502 (2024).

Analytical model of a Tellegen meta-atom

Daria Saltykova[1], Daniel A. Bobylev[1], Maxim A. Gorlach[1]*

[1]School of Physics and Engineering, ITMO University, Saint Petersburg 197101, Russia

corresponding author: m.gorlach@metalab.ifmo.ru

Abstract: Tellegen response is a nonreciprocal effect which couples electric and magnetic responses of the medium and enables unique optical properties. Here, we develop a semi-analytical model of a Mie-resonant Tellegen meta-atom made of magneto-optical material and explicitly compute its magnetoelectric polarizability. We demonstrate that it could substantially exceed the geometric mean of electric and magnetic polarizabilities giving rise to strong and controllable effective Tellegen response in metamaterials.

Tellegen media, originally proposed by B. D. Tellegen [1], occupy a unique place at the intersection of applied photonics and fundamental physics. From a technological perspective, strong magnetoelectric coupling enables the development of compact nonreciprocal components such as isolators, circulators, and topological waveguides [2], which are essential for modern optical systems. From a fundamental perspective, the Tellegen response is closely related to axion electrodynamics [3], offering a laboratory-accessible platform to investigate exotic symmetry-breaking effects. However, in natural materials the effect is typically very weak [4], which makes efficient nonreciprocal wave manipulation unattainable without artificial structures.

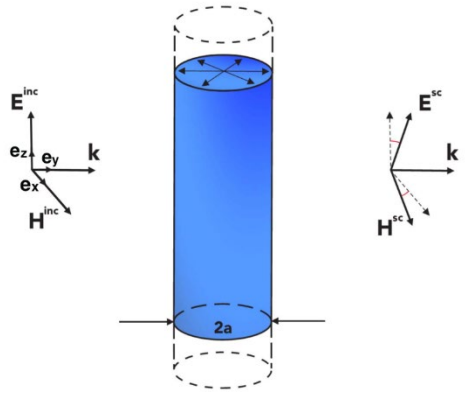

Fig. 1 Scattering of a TM-polarized plane wave by an infinite radially magnetized cylinder of the radius a.

Metamaterials offer a promising solution: by engineering artificial unit cells, one can achieve strong and tunable magnetoelectric response [5]. In this work, we present a semi-analytical model of a Mie-resonant Tellegen meta-atom based on a conventional magneto-optical material. Specifically, we consider a radially magnetized cylinder, schematically shown in Fig. 1, and study its excitation by a TM-polarized plane wave.

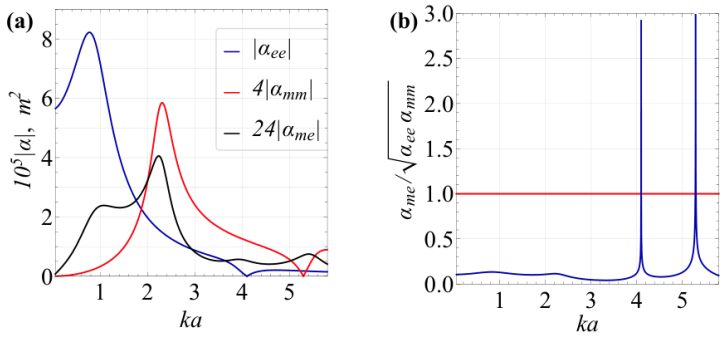

Fig. 2. Frequency dependence of polarizabilities for a radially magnetized gyrotropic cylinder. (a) Electric, magnetic, and magnetoelectric polarizabilities versus normalized frequency ka. Peaks in magnetoelectric coupling coincide with dipole resonances. (b) Dimensionless ratio $|\alpha^{em}| / \sqrt{(|\alpha^{ee}|\cdot|\alpha^{mm}|)}$ as a function of ka, showing that the coupling can exceed the established bound. Parameters: a = 0.005 m, g = 1, ε = 10, μ = 1.

This configuration breaks time-reversal and mirror symmetries in a way that guarantees a pure Tellegen response while suppressing unwanted magneto-optical effects. Using perturbation theory, we derive analytical expressions for the electric, magnetic, and magnetoelectric polarizabilities and analyze their frequency dependence. As illustrated in Fig. 2(a-b), the Tellegen coupling peaks at the dipole resonances and, in certain regimes, even exceeds the previously established theoretical bound [6].

Full-wave numerical simulations confirm the validity of our model and clearly reveal cross-polarized scattered fields, which serve as direct evidence of magnetoelectric coupling. Together, these results show that overlapping dipole resonances offer a practical route to achieving giant Tellegen responses. Our findings provide a solid theoretical framework for the design of Tellegen meta-atoms

and highlight their potential in nonreciprocal wave manipulation, topological photonics, and experimental studies of axion electrodynamics.

Theoretical models were supported by the *Priority 2030 Federal Academic Leadership Program*. Numerical simulations were supported by the *Russian Science Foundation (Grant No. 23-72-10026)*.

References

[1] B. D. Tellegen, *The gyrator, a new electric network element*, Philips Res. Rep. 3, 81 (1948).

[2] F. R. Prudêncio, M. G. Silveirinha, *Optical isolation of circularly polarized light with a spontaneous magnetoelectric effect*, Phys. Rev. A 93, 043846 (2016).

[3] F. Wilczek, *Two applications of axion electrodynamics*, Phys. Rev. Lett. 58, 1799–1802 (1987).

[4] A. P. Pyatakov, A. K. Zvezdin, *Magnetoelectric and multiferroic media*, Phys. Usp. 55, 557–581 (2012).

[5] S. Safaei Jazi et al., *Optical Tellegen metamaterial with spontaneous magnetization*, Nat. Commun. 15, 1293 (2024).

[6] T. Z. Seidov, M. A. Gorlach, *Unbounded Tellegen response in media with multiple resonances*, Phys. Rev. A 111, 033521 (2025).

Enhanced absorption and radiation control in MoS_2 monolayers with periodic nanowire array

E. S. Zavyalova[1,2*], A. D. Bolshakov[1,3]

[1]Moskow institute of physics and technology, Instituusky lane, 9, Dolgoprudny 141701, Russia

[2]ITMO university, Lomonosova street, 9, Saint-Petersburg 191002, Russia

[3]Alferov university, Chlopina street, 8, Saint-Petersburg 194021, Russia

[*]corresponding author: eseniia.zavialova@metalab.ifmo.ru

Abstract: We investigate a hybrid nanophotonic system consisting of a monolayer of MoS_2 and a periodic array of GaP dielectric nanowires. The array is shown to provide significant absorption enhancement in the MoS_2 layer for both incident polarizations (TE and TM). For the TM polarization, a strong increase in the electrical energy density is achieved at large interwire gaps, and at a nanowire diameter of approximately 190 nm, excitation of the quasi-BIC mode is observed, providing resonant field enhancement.

Two-dimensional materials such as MoS_2 exhibit unique optical properties, including pronounced luminescence even at atomic thicknesses. However, their emission efficiency is limited by the small volume of the active layer. Integration with dielectric nanostructures allows for enhanced interaction with light by localizing electromagnetic modes. Periodic arrays of GaP nanowires offer a promising platform due to GaP's low losses in the visible range and flexibility in configuring geometric parameters [1].

A system consisting of a 0.7 nm thick MoS_2 monolayer placed under a one-dimensional array of GaP dielectric nanowires was considered. The gap between the nanowires varies from 10 to 250 nm, and the diameter (D) of the nanowires ranges from 100 to 300 nm. The impact of these parameters on absorption in the monolayer is explored in two different polarizations. The excitation wavelength is 532 nm (Fig. 1).

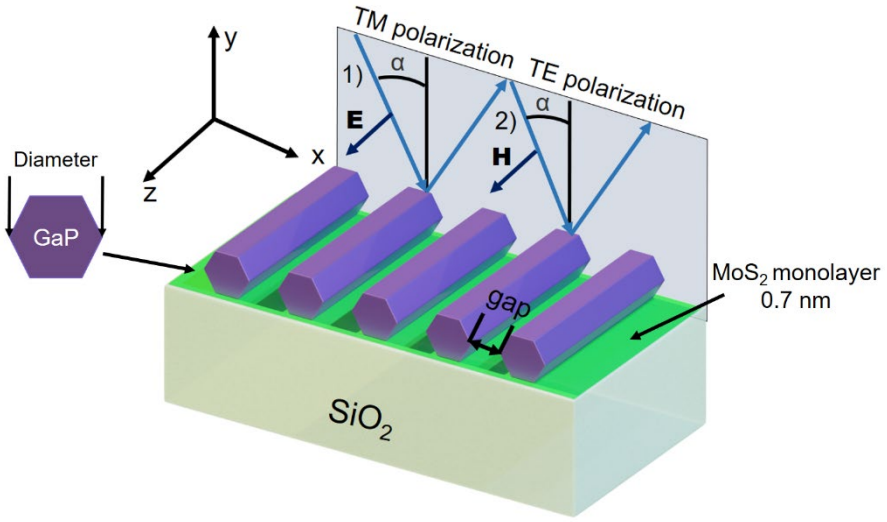

Fig. 1 Model geometry for the numerical simulation

The presence of a periodic array of nanowires leads to enhanced absorption in the MoS_2 layer compared to the isolated case with two polarizations (Fig. 2). This enhancement is due to the excitation of certain collective modes, which lead to an increase in the local electromagnetic energy density. For TE polarization, the gain is achieved at small gaps, whereas for TM polarization, an increase in energy density is possible at large gaps between nanowires.

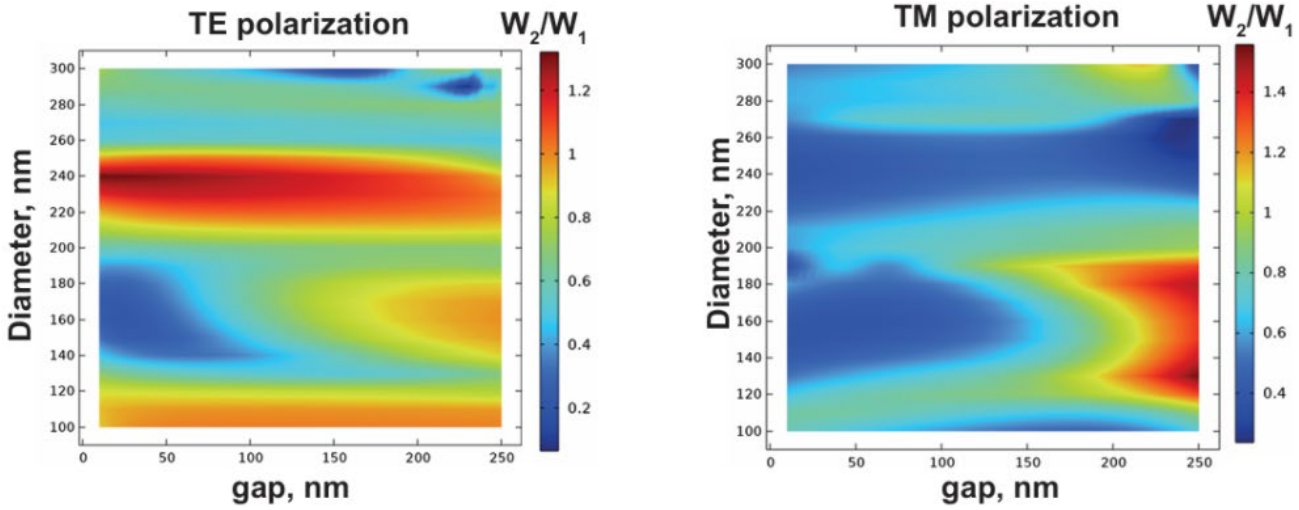

Fig. 2 Maps of electric energy density (W) depending on gap and diameter (W_2 – electric energy density with a periodic array, W_1 – electric energy density without a periodic array)

Of particular interest is the case of TM polarization at nanowire diameters of ~190 nm, where excitation of the quasi-bound state in the continuum (quasi-BIC) is observed (Fig. 3). This mode provides a resonant enhancement of the electric field and, consequently, a significant increase in absorption in the MoS_2 layer.

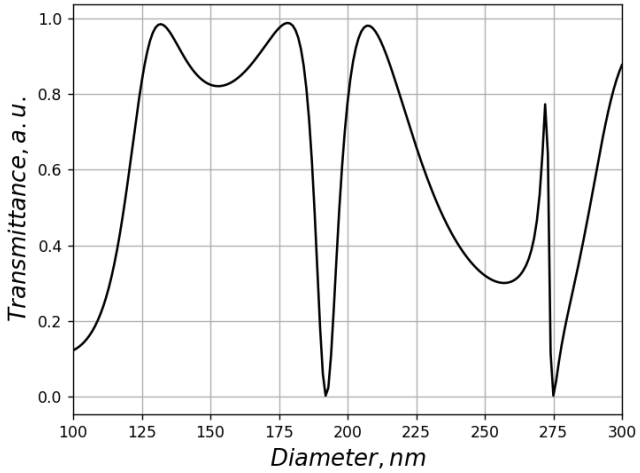

Fig. 3 Dependence of transmission on the diameter for the gap = 200 nm

The obtained results show that the integration of a MoS_2 monolayer with a GaP nanowire array allows for effective enhancement of absorption and control of emission depending on the polarization and geometric parameters of the array.

This work is supported by the Russian Science Foundation (Grant No. 24-12-00225)

References

[1] D. E. Aspnes, A. A. Studna, Phys. Rev. B Condens. Matter., **27**, 985 (1983).2.

Designing a High-Performance NO_2 Optical Fiber Sensor by Revealing the Key Characteristics of Single-Walled Carbon Nanotube Films

Egor O. Zhermolenko[1]*, Khasan A. Akhmadiev[1], Aram A. Mkrtchyan[1], Fedor S. Fedorov[1], Anastasiia S. Netrusova[1], Aliya R. Vildanova[1], Dmitry V. Krasnikov[1], Albert G. Nasibulin[1] and Yuriy G. Gladush[1]

[1]Skolkovo Institute of Science and Technology, the territory of the Skolkovo Innovation Center, Bolshoy Boulevard, 30, bld. 1, Moscow 121205, Russia

*corresponding author: egor.zhermolenko@skoltech.ru

Abstract: We developed a novel optical fiber sensor for nitrogen dioxide (NO_2) detection by integrating side-polished fibers with single-walled carbon nanotube (SWCNT) films. This design establishes a receptor-transducer methodology where the SWCNTs' optoelectronic properties are modulated by NO_2 adsorption. The achieved sensor exhibits a robust limit of detection of 400 ppb and offers significant advantages for harsh industrial environments, including inherent corrosion resistance, electromagnetic immunity, and compatibility with existing telecom infrastructure.

The increasing levels of industrial emissions require sophisticated environmental monitoring, especially for corrosive pollutants such as NO_2. Its oxidizing nature allows it to form corrosive acids

(HNO_2/HNO_3) when hydrated and presents substantial health threats even at low levels. Strict exposure limits are mandated by regulatory agencies: a TLV-TWA of 500 ppb[1], and an annual average concentration of 5.2 ppb as reported by the WHO.[2] Existing technologies like electrochemical sensors, pellistors, and metal oxide sensors degrade quickly in these corrosive environments, creating a critical need for more durable solutions. Although carbon nanomaterial-based resistive sensors (e.g., using graphene or SWCNTs) provide excellent sensitivity[3], they are susceptible to electromagnetic interference. Optical fiber sensors address these shortcomings with their intrinsic corrosion resistance and immunity to electromagnetic fields, alongside benefits including remote operation[4], minimal power needs[5], low-noise performance[6], and the ability to be selectively tuned to specific wavelengths.

To leverage these properties for NO_2 sensing, we created a new evanescent wave sensor that combines side-polished fibers with SWCNT films. This configuration implements a receptor-transducer design philosophy in which the SWCNT receptor material is specifically optimized to work in synergy with the fiber-optic transducer. The detection principle utilizes NO_2-induced changes to the optoelectronic characteristics of the SWCNTs: adsorption modifies intra-nanotube bandgaps through charge transfer doping. A key finding is that peak performance depends on precisely matching the SWCNT S_{11} optical transition with the 1550 nm telecom window to enhance evanescent field interaction, while also carefully controlling film thickness to achieve a balance in evanescent wave penetration depth.

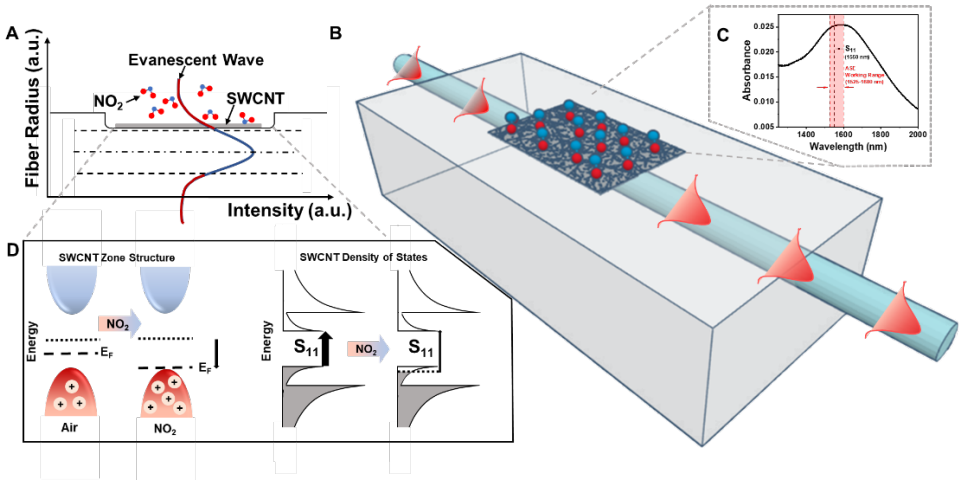

Fig. 1. A) Illustration of the interaction mechanisms between analyte, evanescent field and SWCNT placed on SPF. B) D-Shape embedded in a quartz block with SWCNT film deposited on the polished region. C) Absorption spectrum of SWCNT film. D) Schematic zone structure and density of states in semiconducting SWCNTs.

Experimental results demonstrated an optical detection limit of 400 ppb, a sensitivity of 0.004 dB/ppm, and response/recovery times of 8.6 and 18.5 minutes, respectively. The sensor's fully fiber-based design requires no free-space optical components, improving its durability for harsh industrial settings, and its compatibility with telecom standards allows for integration into established infrastructure.

This project was supported by the Russian Science Foundation (Grant No. 22-13-00436 (П)).

References

[1] European Parliament; European Council, *Official Journal of the European Communities* 2008, *152*.

[2] European Commission, *Recommendation from the Scientific Committee on Occupational Exposure Limits for Nitrogen Dioxide*, 2014.

[3] Schedin, F., Geim, A. K., Morozov, S. V., Hill, E. W., Blake, P., Katsnelson, M. I., & Novoselov, K. S. "Detection of individual gas molecules adsorbed on graphene." Nature materials 6.9 (2007)

[4] Sabbah, S., Harig, R., Rusch, P., Eichmann, J., Keens, A., & Gerhard, J. H. "Remote sensing of gases by hyperspectral imaging: system performance and measurements." Optical Engineering 51.11 (2012)

[5] Cho, I., Sim, Y. C., Cho, M., Cho, Y. H., & Park, I. "Monolithic micro light-emitting diode/metal oxide nanowire gas sensor with microwatt-level power consumption." ACS sensors 5.2 (2020)

[6] X. Zhao, C. Li, H. Qi, J. Huang, Y. Xu, Z. Wang, X. Han, M. Guo, K. Chen. "Integrated near-infrared fiber-optic photoacoustic sensing demodulator for ultra-high sensitivity gas detection." Photoacoustics 33 (2023)

All-dielectric layered structures for vectorial spatial differentiation of optical beams

A. I. Kashapov[1,2*], E. A. Bezus[1,2], D. A. Bykov[1,2] and L. L. Doskolovich[1,2]

[1]Image Processing Systems Institute, National Research Centre "Kurchatov Institute", Molodogvardeyskaya St., 151, Samara 443001, Russia

[2]Samara National Research University, Moskovskoe shosse, 34, Samara 443086, Russia

[*]corresponding author: ar.kashapov@gmail.com

Abstract: We propose an all-dielectric three-layer structure for the optical implementation of vectorial spatial differentiation. Numerical simulations show that the reflected intensity closely matches the squared magnitude of the incident beam gradient with error below 1%. The results highlight the potential of the presented structure for compact photonic devices for analog optical computing and real-time image processing.

The optical implementation of vectorial spatial differentiation using an all-dielectric three-layer structure with an M-shaped refractive index profile (hereafter referred to as the M-structure) (see the inset in Fig. 1) is considered. Unlike the well-studied W-structures [1,2], which enable efficient differentiation only along a single transverse axis, the designed M-structure provides "balanced" transfer functions for both transverse field components, thereby allowing isotropic vectorial differentiation. This design thus enables compact photonic differentiators with potential applications in analog image processing.

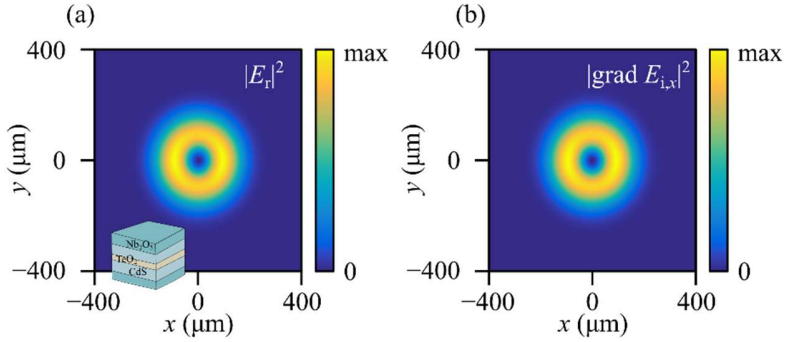

Fig. 1 (a) Reflected intensity distribution obtained by numerical simulation; (b) analytically calculated squared absolute value of the gradient of the incident beam. The inset shows the geometry of the three-layer M-structure.

The operation of the proposed structure relies on the occurrence of a reflection zero at a given wavelength and angle of incidence, which can be obtained by adjusting the thickness of the central and cladding layers. As a proof of concept, we designed a structure composed of a TeO_2 core, CdS claddings, and Nb_2O_5 as the surrounding medium, optimized for operation at a wavelength of 630 nm and an incidence angle of 41.5°. For an incident Gaussian beam with a 10-μm waist, the profiles of the transverse components of the reflected field (rigorously calculated using the method described in [3]) closely match the analytical first-order derivatives of the input beam profile. The normalized root-mean-square deviation (RMSD) of calculating the squared gradient is below 1%, indicating good performance of the designed structure. Furthermore, tolerance analysis shows that small deviations in layer thickness (±1 nm) or incidence angle (±0.5°) do not significantly degrade the differentiation quality, demonstrating robustness

with respect to fabrication and alignment errors. In Fig. 1, the numerically calculated reflected intensity distribution is compared with the analytically calculated squared absolute value of the gradient of the incident beam, showing excellent agreement between them.

In conclusion, we investigated the implementation of vectorial spatial differentiation using an all-dielectric three-layer structure with an M-shaped refractive index profile. Numerical simulation results confirmed that the designed structure provides nearly balanced responses for both transverse field components, allowing isotropic vectorial differentiation. Simulations with a Gaussian input beam showed good agreement with analytical predictions and demonstrated the feasibility of this approach. The results indicate that such layered structure can be used for analog optical signal processing, including edge detection and related image analysis tasks.

This work is supported by the Ministry of Science and Higher Education of the Russian Federation (state assignment to Samara University FSSS-2024-0016).

References

[1] Golovastikov, N.V., Doskolovich, L.L., Bezus, E.A., Bykov, D.A., & Soifer, V.A., "An optical differentiator based on a three-layer structure with a W-shaped refractive index profile," J. Exp. Theor. Phys., **127**, 202–209 (2018).

[2]. Kawakami, S. & Nishida, S., "Characteristics of a doubly clad optical fiber with a low-index inner cladding," IEEE J. Quantum Electron., **10(12)**, 879–887 (1974).

[3] Moharam, M.G., Pommet, D.A., Grann, E.B., & Gaylord, T.K., "Stable implementation of the rigorous coupled-wave analysis for surface-relief gratings: enhanced transmittance matrix approach," J. Opt. Soc. Amer. A, **12(5)**, 1077–1086 (1995).